University of Thi-Qar Journal of Science (UTJsci)
E-ISSN: 2709-0256, P-ISSN: 1991-8690, Vol. 13, No. 1, Jun. 2026

# Spray-Pyrolyzed Thin Films of GO, $TiO_2$, ZnO, and $SnO_2$: A Comparative Structural and Morphological Study

Mustafa Al-Shuwaili*[1a], Hayder Mousa Neamah[2b], Hayder Mohsin Jasimand[3c] and Mahdi Hdidar[4d]

[1]*Department of physics, College of Science, University of Thi-Qar, 64001, Iraq*
[2]*College of Education, Department of Physics, University of Al-Qadisiyah, Iraq*
[3]*College of Basic Education, Al-Mustansiriya University, Iraq*
[4]*Laboratory of Ceramics Composites and Polymer Materials (LaMaCoP), Faculty of sciences of Sfax, University of Sfax, Tunisia*.

[b]E-mail: Hayder.mosa@qu.edu.iq
, [c]E-mail: haider_mohsen1993@uomustansiriyah.edu.iq, [d]E-mail :mahdi.hdidar@fss.usf.tn

[a*]Corresponding author: mustafa.khaleel.ph@utq.edu.iq

Received: 13-04-2026, Revised: 30-05-2026, Accepted: 31-05-2026, Published: 01-06-2026

***Abstract*—This study examined the optical characteristics of graphene oxide (GO) and its nanocomposites ($GO@TiO_2$, GO@ZnO, and $GO@SnO_2$). The nanocomposites were prepared using a hydrothermal method. X-ray diffraction (XRD), energy-dispersive X-ray spectroscopy (EDX), and atomic force microscopy (AFM) were used to investigate the structure and morphology of the materials.**

**The XRD diffractograms confirmed the successful integration of metal nanoparticles onto GO sheets. For GO@ZnO, characteristic diffraction peaks confirmed the presence of ZnO nanoparticles. For $GO@SnO_2$, peaks corresponding to crystallographic planes (110), (101), (200), (211), (220), and (112) confirmed the $SnO_2$ phase. For $GO@TiO_2$, peaks associated with planes (001), (101), (004), (200), and (110) confirmed the $TiO_2$ phase. The pictures seen in the crystallographic plans (110), (101), (200), (211), (220), and (112) for the nanocomposite $GO@SnO_2$ confirm the creation of the phase $SnO_2$. Furthermore, the development of the $GO@TiO_2$ nanocomposite is confirmed by the images associated with plans (001), (101), (004), (200), and (110), which are characteristic of the phase $TiO_2$. EDX analysis revealed the presence of oxygen-containing groups characteristic of GO and confirmed the incorporation of metal oxide nanoparticles within the nanocomposites. AFM investigations showed that the introduction of nanoparticles resulted in a decrease in surface roughness and altered the topography of GO sheets. FESEM images further confirmed the morphological changes, showing spherical ZnO nanoparticles, leaf-like $SnO_2$ structures, and agglomerated $TiO_2$ grains on GO surfaces.**

***Keywords*—Graphene Oxide, GO nanocomposites, metal oxide, thin film, spray pyrolysis.**

## I. INTRODUCTION

Due to their exceptional mechanical, electrical, thermal, and barrier properties, graphene-based nanocomposites have experienced rapid growth during the past ten years [1]. Among the graphene derivatives, graphene oxide (GO) and graphene oxide reduced (rGO) stand out as promising candidates for nanocomposite applications, particularly due to their synthetic and extendable nature using descendent (top-down) approaches [2]. These materials have expanded the field of nanocomposites and contributed to significant advancements in this field.

Since its separation by Andre Geim and Konstantin Novoselov in 2004, graphs have taken center stage in material science research. On the structural level, it is a two-dimensional (2D) allotrope of carbon in which each atom contributes to a localized π, giving this material remarkable physical properties [3]. The graphene has a Young module of about 1 TPa, high electrical conductivity, exceptional charge carrier mobility, high thermal conductivity, and a large specific surface area (~2630 $m^2 \cdot g^{-1}$) [4]. These unique characteristics make graphene and its derivatives appealing for a variety of technological applications, including flexible electronics, energy storage systems, capacitors, optoelectronic devices, and biomedicine [5].

The materials derived from graphene have been extensively investigated for advanced applications, such as transparent conductive electrodes, flexible electrodes, hydrogen storage systems, high-speed electronic devices, and biocapteurs [6].

In the biomedical field, they have been investigated for the reinforcement of biodegradable materials used in osseous and tissue engineering, as well as for medication administration and cicatrisation [7]. Recent research focuses on integrating graphene derivatives with metallic oxides to create nanocomposites with improved physicochemical properties.

For instance, adding rGO to small TiO2 sofas improves their structural, optical, and functional properties. In this connection, A.S. AlShammari et al. (2020) [8] deposited small $TiO_2$/rGO couches via pyrolysis by aérosol on oxygen-doped fluor (FTO) substrates, demonstrating the impact of GO teneur on crystallinity, morphology, and optical properties. Additionally, $TiO_2$–rGO composites have been extensively studied for photocatalytic applications,


https://doi.org/10.32792/utq/utjsci/v13i1.1618

such as hydrogen synthesis using solar energy, where the amount of rGO plays a crucial role in improving light absorption and charge separation efficiency [9].

Furthermore, the synthesis of GO-oxide metal nanocomposites is frequently reported. According to R.P. Reshma et al. (2024) [10]. GO and $SnO_2$ nanoparticles can be produced via coprecipitation and modified Hummers methods, respectively, while GO–$SnO_2$ nanocomposites are often separated by hydrothermal means. Oxide metal and graphene oxide nanocomposites (TMO/GO), including those based on $SnO_2$, are a type of polyvalent materials that combine the redox activity of metal oxides with the electrical conductivity and mechanical robustness of graphene derivatives. This synergy makes them particularly suited for applications in energy storage, catalysis, and environmental remediation [11].

Recent developments have highlighted the potential of graphene-based nanocomposites for biodetection platforms of biomolecules, heavy metals, and disease biomarkers [12], as well as for drug delivery systems in cancer and tissue engineering [13]. Despite these advancements, there are still concerns about the long-term stability of these nanocomposites for practical and commercial uses [14].
Additionally, because of their simplicity, polyvalence, and effectiveness, hydrothermal approaches have been widely used for the synthesis of nanocomposites based on metal oxides and graphene [15]. Thus, pure $SnO_2$ nanoparticles and $SnO_2$–rGO nanocomposites were synthesized using a hydrothermal monobloc method[16]. These investigations provide important information about the structural, morphological, compositional, optical, and vibrational properties of synthetic materials.

More recently, Rasha S. Yousif (2025) [17] reported on the development of graphene oxide (GO)-based nanocomposites containing ZnO and SnO2 nanoparticles, paying particular attention to their structural, morphological, and autonetoyant characteristics. In this work, GO was prepared using a modified Hummers method and then linked to ZnO and $SnO_2$ nanoparticles. The resulting nanocomposites were deposited as small couches on verre substrates by pyrolysis by pulverization, demonstrating the versatility of this technique for the development of functional revisions.

The results showed that the hydrophobicity of GO–$SnO_2$ nanocomposites is higher than that of GO pure and GO–ZnO systems, highlighting their potential for use as protective and autonetoyant materials [17]
Additionally, Zahraa M. Talib and her associates (2022) [18] investigated small couches of graphene-ZnO hybrids prepared by pyrolysis by pulverization at 350 °C, varying the concentration of graphene nanoplaquettes (from 0.1 to 0.5% in mass). X-ray diffraction (XRD) analysis revealed a polycristalline hexagon-shaped wurtzite structure without the detection of secondary phases.

Additionally, the addition of graphene has significantly changed some important structural parameters, such as the size of crystals, the density of dislocations, and microdeformations. Examining the surface morphology has shown that the teneur in graphene plays a significant role in controlling the growth of grains and the alteration of ZnO's microstructure.

Also, optical characterizations have shown an increase in the interdite band size, from 3.4 eV for pure ZnO to 2.7 eV as graphene concentration increases, confirming the graphene's effectiveness in interdite band modulation [18].
In a different study, Chunyu Ma et al. (2021) described the synthesis of small GO-$TiO_2$ couches modified by silver nanoparticles using sol-gel and centrifugation procedures. A controlled cathodic pulverization procedure has made it possible to obtain a uniform distribution of metal nanoparticles with sizes ranging from 23 to 51 nm on the film's surface. All of which improved photocatalytic activity. Similar studies have shown that the Ag-modified $TiO_2$-GO nanocomposites exhibit increased photocatalytic activity due to improved charge separation and surface plasmonic resonance effects, even though the precise results have not been fully verified [19–21].

The aim of this work is to synthesize graphene oxide (GO) and its nanocomposites with ZnO, $SnO_2$, and $TiO_2$ via a hydrothermal method, and to investigate their structural, morphological, and topographical properties using XRD, AFM, and FESEM. Unlike previous studies, this research focuses on comparing the morphological changes induced by different metal oxide nanoparticles on GO sheets under identical synthesis conditions, providing new insights into the surface roughness and crystallite size variations.

## II. THE EXPERIMENTAL METHOD

### A. Material Synthesis

All highly pure reagents were purchased from Merck (Germany) and used without further purification. Graphite powder (99.9%), sulfuric acid ($H_2SO_4$, 98%), phosphoric acid ($H_3PO_4$, 85%), potassium permanganate ($KMnO_4$, 99%), hydrogen peroxide ($H_2O_2$, 30%), zinc nitrate hexahydrate ($Zn(NO_3)_2{\cdot}6H_2O$, 99%), sodium hydroxide (NaOH, 98%), tin(IV) chloride pentahydrate ($SnCl_4{\cdot}5H_2O$, 98%), and titanium tetrachloride ($TiCl_4$, 99%) were used.

### B. Making the graphene oxide (GO) solution

The modified Hummers method was used to synthesize graphene oxide from natural graphite paillettes. at a standard procedure, 2.0 g of graphite paillettes were added to a mixture of sulfuric acid (H2SO4) and phosphoric acid ($H_2PO_4$) at a volumetric ratio of 9:1 (180 mL:20 mL) while being continuously stirred in a glass container for two hours. After that, 7.3 g of potassium permanganate ($KMnO_4$) was gradually added to the mixture while the temperature was kept above 10 °C and stirred continuously for 48 hours. Over time, 90 milliliters of distilled water were gradually added with quick stirring, which caused the mixture's color to change from brown to yellow and a suspension to form. Then, 7.0 mL of hydrogen peroxide ($H_2O_2$) and 55 mL of distilled water were used to convert the residual manganese oxides and permanganate into manganese sulfate.

### C. Making the GO@ZnO solution

The GO@ZnO nanocomposite was prepared in batch using a hydrothermal method. The precursors used were zinc nitrate hexahydrate ($Zn(NO_3)_2{\cdot}6H_2O$) and sodium hydroxide (NaOH) ($Zn(NO_3)_2{\cdot}6H_2O$) and sodium hydroxide

(NaOH), which are linked to the previously synthesized graphene oxide. In a standard procedure, a suitable mass of GO (dispersed in 100 mL of mineralized water) was mixed with a solution containing 5 mmol of $Zn(NO_3)_2 \cdot 6H_2O$ and 10 mmol of NaOH under magnetic stirring. To ensure a uniform dispersion, the mixture was subjected to ultrasonication for 30 minutes. The resulting solution was transferred to an autoclave made of inoxydable iron with a Teflon liner. The reactor was naturally cooled to room temperature after being heated to 180 °C for 24 hours. Filtration was used to recover the solid product, which was then repeatedly exposed to demineralized water and heated to 80 °C for 15 hours. The resulting powder has been named GO@ZnO.

### *D. Making the GO@$SnO_2$ solution*

The nanocomposite GO@$SnO_2$ was synthesized using a method similar to that of GO@ZnO, substituting the zinc precursor with tin(IV) chloride pentahydrate ($SnCl_4 \cdot 5H_2O$). Briefly, a GO dispersion (prepared as described in 2.1.1) was mixed with an aqueous solution containing 10 mmol of NaOH and 5 mmol of $SnCl_4 \cdot 5H_2O$. After 30 minutes of ultrasonication, the mixture was placed in an autoclave made of inoxydable iron with a Teflon liner. The hydrothermal treatment was carried out at 180 °C for 24 hours, followed by a natural cooling process. The precipitate was filtered, exposed to a lot of demineralized water, and then heated to 80 degrees Celsius for 15 hours. The final material is GO@$SnO_2$.

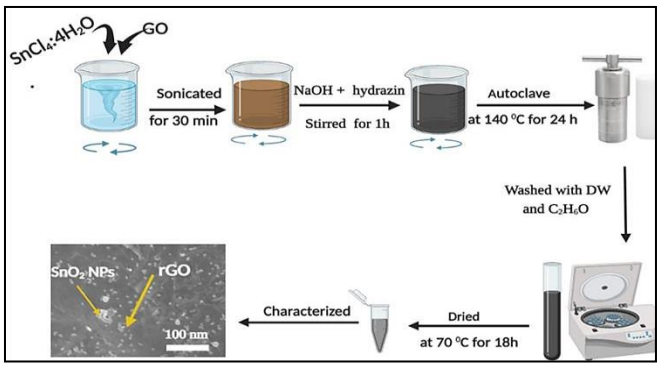

Fig. 1: Schematics of the $SnO_2$-rGO NCs synthesis [15].

### *E. GO@$TiO_2$ solution preparation.*

The GO@$TiO_2$ nanocomposite was prepared using a hydrothermal method in a similar batch. Due to their controlled reactivity in an aqueous environment, the precursor of titanium is either the isopropoxide of titanium ($Ti(OCH(CH_3)_2)_4$) or the titanium tetrachloride ($TiCl_4$). In a standard procedure, a dispersion of GO (100 mL, containing around 50 mg of GO) was mixed with 5 mmol of $TiCl_4$ diluted in ethanol to prevent an overly quick hydrolysis.
To bring the pH down to about 10, a solution of NaOH (10 mmol in 20 mL of water) was added drop by drop while being stirred. After 30 minutes of ultrasonication, the mixture was placed in an autoclave made of inoxydable iron with a Teflon liner. The temperature was raised to 180 °C for 24 hours and then naturally cooled. The product was filtered, repeatedly exposed to ethanol and demineralized water, and then heated to 80 °C for 15 hours. The resulting nanocomposite is known as GO@$TiO_2$.After that, 7.3 g of potassium permanganate ($KMnO_4$) was gradually added to the mixture while the temperature was kept above 10 °C and stirred continuously for 48 hours. Over time, 90 milliliters of distilled water were gradually added with quick stirring, which caused the mixture's color to change from brown to yellow and a suspension to form. Then, 7.0 mL of hydrogen peroxide ($H_2O_2$) and 55 mL of distilled water were used to convert the residual manganese oxides and permanganate into manganese sulfate.

### *F. Thin film deposition*

Before thin film deposition, glass substrates were ultrasonically cleaned in ethanol and distilled water for 30 minutes each [22]. Using compressed air as the carrier gas and a 35 mL solution volume, spray pyrolysis was used to deposit the films. The spray settings comprised a deposition rate of 2–2.5 mL/min and a nozzle-to-substrate distance of roughly 30–40 cm[23]. For GO, GO@ZnO, GO@$SnO_2$, and GO@$TiO_2$ thin films, substrate temperatures were tuned at 50, 150, 400, 500, and 550 °C, respectively, in line with the usual temperature ranges employed for these materials' development via spray pyrolysis.

## III. Results

### *A. Structural characterization by X-ray diffraction (XRD)*

X-ray diffraction (XRD) is a preferred method for analyzing the crystal structure of materials. Its foundation is the diffusion of a beam of X rays by a crystal's atoms, resulting in certain diffraction patterns. By recording the angles and intensities of these images, it is possible to reconstruct the electron density map inside the crystal, which allows one to determine the average atomic locations, their chemical relationships, and any potential structural disorders.
Fig. 1 shows the XRD patterns of pure graphene oxide (GO) and nanocomposites containing ZnO, $SnO_2$, and $TiO_2$. On Fig.2 (a), the non-modified GO displays a well-defined diffraction picture at $2\theta = 11°$. In general, two types of crystals are distinguished: true crystals, which are ordered over a long distance, and amorphous or pseudocrystals crystals, which are ordered over a short distance. The first ones show sharp and intense diffraction images with distinct phases. On the other hand, pseudo crystals produce larger images. In the case of GO, the atoms are arranged according to a type AB empilement, and the size of the leaves varies according on the degree of oxidation. The picture at $2\theta \approx 11°$ corresponds to plan (001) and is attributed to the presence of functional oxygenated groups. A second, larger image, at $2\theta = 24°$, is associated with residual graphite in the GO and comes from the plan (002).
The XRD pattern of the GO@ZnO nanocomposite (Fig. 2 (c)) shows a broad peak at $2\theta = 24°$, indicating the interaction between ZnO nanoparticles and the GO matrix. This peak confirms the incorporation of ZnO into the nanocomposite structure. into the nanocomposite's structure.
Regarding the GO@$SnO_2$ nanocomposite (Fig. 2(d)), diffraction images appear at $2\theta = 26{,}35°$; 33,7°; 37,65°;

51,6°; 54,8°; and 65,8°. These images are attributed to the crystal plans (110), (101), (200), (211), (220), and (112) of the $SnO_2$ phase, confirming the presence of oxygen in the GO matrix.

TABLE 1. Crystallite size and FWHM of nanoparticles.

| Sample | Peak (2θ) | FWHM (deg) | Crystallite size (nm) |
|---|---|---|---|
| GO@$SnO_2$ | 26.35° | 0.45 | 18.2 |
| GO@$TiO_2$ | 25.4° | 0.52 | 15.6 |

The XRD pattern of GO@$TiO_2$ Fig. 1(d) shows a peak at 2θ = 10.76° corresponding to the (001) basal plane of GO, confirming its presence in the composite. Using Bragg's law (nλ = 2d sinθ), the interlayer spacing (d) was calculated to be 0.82 nm, which is larger than that of pure GO due to the intercalation of $TiO_2$ nanoparticles. Additionally, peaks at 2θ = 25.4°, 37.96°, and 48.36° correspond to the (101), (004), and (200) planes of the anatase phase of titanium dioxide, confirming the successful formation of the GO@$TiO_2$ nanocomposite bragg, confirming the successful production of the nanocomposite GO@$TiO_2$. The average size of the $TiO_2$ particles was measured at 1,06 Å.

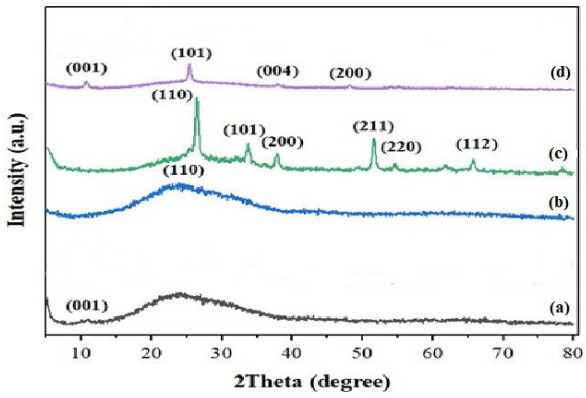


Fig.2. The XRD patterns of (a) bare GO ,(b) GO@Zn, (c) GO@$SnO_2$, (d) GO@$TiO_2$

### *B. Atomic force microscopy (AFM) analysis*

Fig. 3(a,b) shows the GO's unmodified AFM images. The GO sheets have smooth surfaces and are free of any specific contaminants. On the GO's surface, no particle is visible. These findings are consistent with electron microscopy at scanning (FESEM) studies, which also show separate GO sheets.

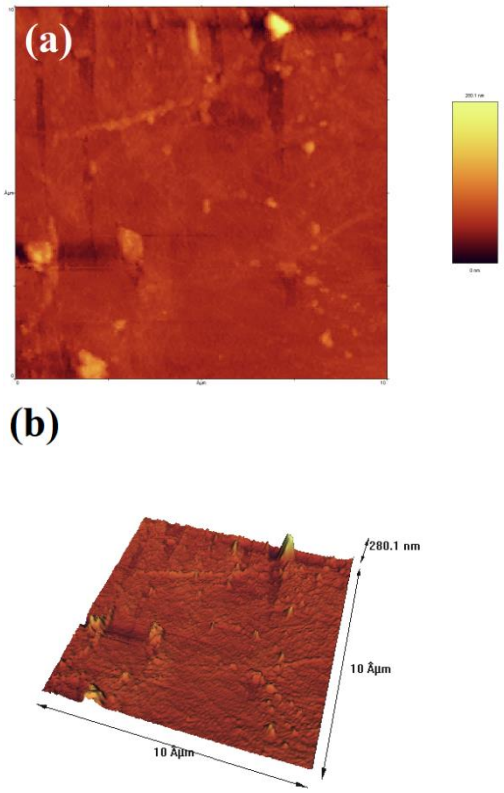


Fig. 3. AFM topographic and their 3D images of the (a,b) bare GO

The AFM image of the Zn@GO nanocomposite is shown in Fig. 3(c,d). The surface of GO is covered with quasi-spherical nanoparticles that have been assimilated into zinc particles. These same nanoparticles were seen in FESEM as spherical grains, confirming the successful production of the nanocomposite. The addition of zinc nanoparticles alters not only the GO's morphology but also reduces its surface roughness.

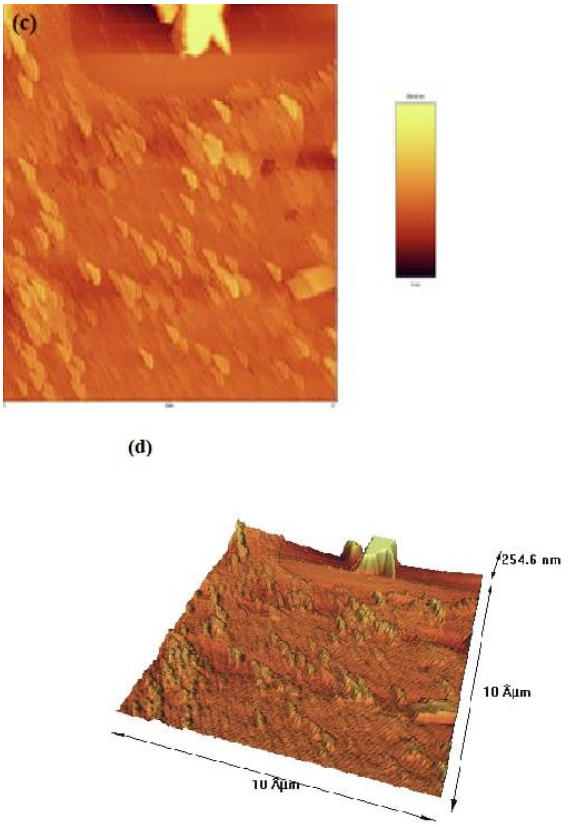


Fig. 3. AFM topographic and their 3D images of the (c,d) GO@Zn

As shown in the AFM image of the nanocomposite $SnO_2$@GO(Fig. 3(e,f), the surface of the material has uniformly distributed spherical grains. These grains are attributed to $SnO_2$ nanoparticles, which have a leaf-like morphology under FESEM microscopy. As observed from the AFM images, the addition of SnO2 nanoparticles increases the structural defects of GO, which affects its rugosity.

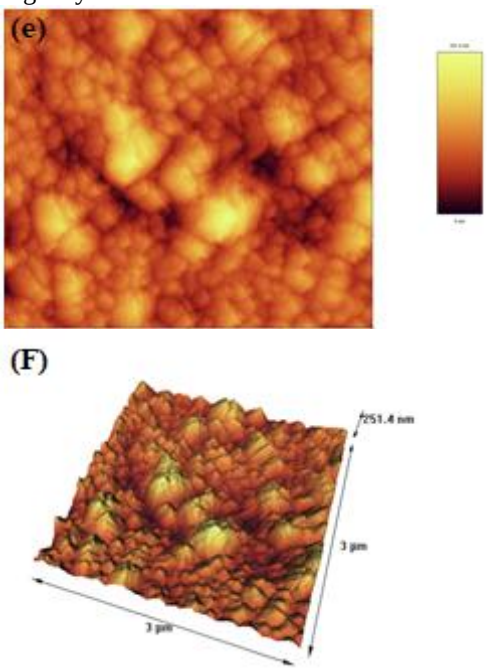


Fig. 1-3. AFM topographic and their 3D images of the (e,f) GO@$SnO_2$

Regarding the AFM image of the nanocomposite $TiO_2$@GO (Fig. 1-3-g,h), the nanoparticles of $TiO_2$ exhibit an agglomeration with a fine morphology that is comparable to that seen in FESEM. Thus, anatase-finished $TiO_2$ granules are detected on the GO surface. The addition of $TiO_2$ nanoparticles increases structural defects within the nanocomposite, which results in a decrease in surface roughness .

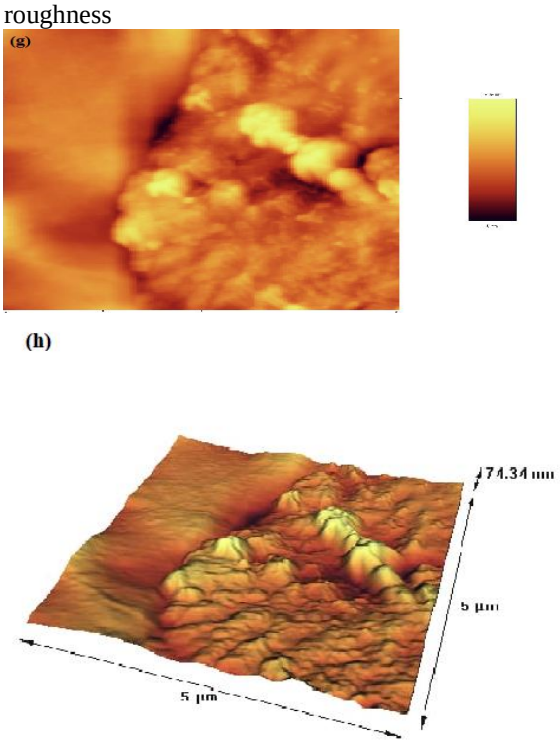


Fig. 3. AFM topographic and their 3D images of the (g,h) GO@$TiO_2$

TABLE 2. Surface roughness parameters from AFM.

| Sample | Average Roughness (Ra, nm) | RMS Roughness (Rq, nm) |
|---|---|---|
| Bare GO | 12.4 | 15.2 |
| GO@ZnO | 8.7 | 10.5 |
| GO@$SnO_2$ | 6.9 | 8.3 |
| GO@$TiO_2$ | 7.5 | 9.1 |

### *C. Field emission scanning electron microscopy (FESEM) analysis*

Fig. 4 summarizes the pictures of GO pure and GO-based nanocomposites containing ZnO, $SnO_2$, and $TiO_2$, respectively, obtained by electron microscopy scanning to field emission (FESEM). FESEM microscopy is a method tailored to the analysis of material morphology. By balancing the surface of the sample with the help of a focused electron beam, it enables the acquisition of high-resolution and very precise pictures for objects ranging in size from micrometers to nanometers. The FESEM images provide useful information about the composition and topography of the samples.

Fig. 4(a) shows the GO's unmodified FESEM picture. There are clearly visible sheets of graphene oxide that are smooth and clean.

The FESEM picture of the GO@ZnO nanocomposite is shown in figure 1-4-b. This material has a crust-like (crust-like) morphology. In addition to these crust-like particles, there are also quasi-spherical nanoparticles scattered on the surface of GO sheets. These spherical particles are attributed to zinc oxide (ZnO) nanoparticles, which range in size from 10 to 40 nm.

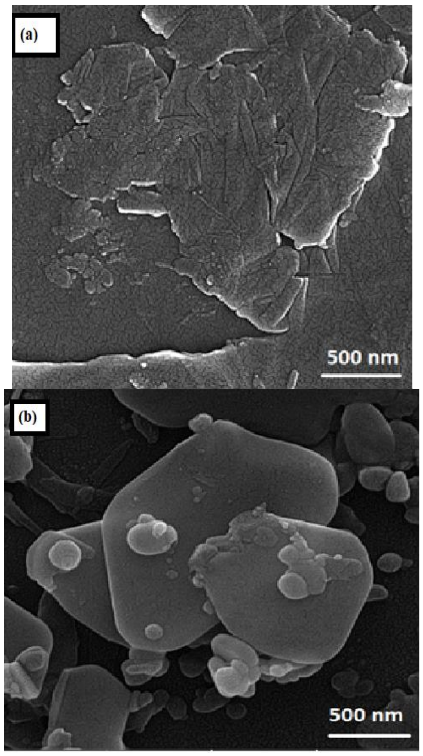


Fig 4-1. The FESM images of (a) bare GO, (b) GO@Zn

The FESEM picture of the GO@$SnO_2$ nanocomposite is shown in Fig.4(C). This material exhibits a leaf-like morphology. The average size of $SnO_2$ nanoparticles is about 200 nm. The comparison of the FESEM images of GO pure and GO@$SnO_2$ revealed that the GO sheets' surface is covered with $SnO_2$ nanoparticles.

The FESEM picture of the nanocomposite GO@$TiO_2$ (figure 1-4-d) shows spherical agglomerated $TiO_2$ grains scattered across the GO surface. These nanoparticles have a rather uniform size, averaging 50 nm.

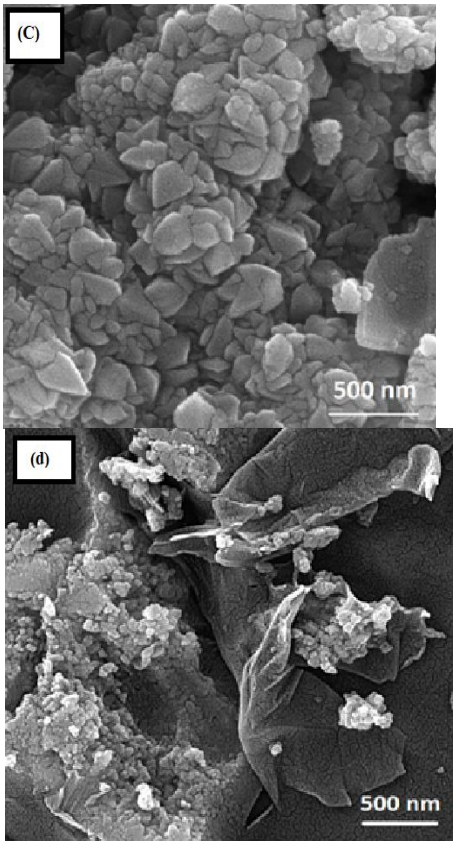


Fig.4 The FESM images of (c) GO@$SnO_2$, (d) GO@$TiO_2$

## IV. Conclusions

This study examined the morphological behavior of graphene oxide (GO) and its nanocomposites (GO@ZnO, GO@$SnO_2$, and GO@$TiO_2$). The successful synthesis of these nanocomposites has been confirmed by the results of investigations using X-ray diffraction (XRD), electron microscopy with balayage to emission of champ (FESEM), and atomic force microscopy (AFM).

Regarding the diffraction of X-rays, the crystal plans (110) have demonstrated the adhesion of zinc nanoparticles to the GO surface. Plans (110), (101), (200), (211), (220), and (112) confirm the presence of $SnO_2$ nanoparticles inside the structure of the GO@$SnO_2$ nanocomposite. Additionally, the production of the nanocomposite GO@$TiO_2$ is confirmed by the crystal plans (001), (101), (004), (200), and (110).

The AFM and FESEM images have demonstrated that the nanocomposites' morphologies are clearly unique, providing additional evidence of their synthesis. Additionally, AFM tests have shown that the addition of metal nanoparticles results in a decrease in surface roughness.

## Conflict of interest

Authors declare that they have no conflict of interest.

REFERENCES


[1] M.K. Araújo, A.S. Carvalho, A.R. Santos, E. Padrón-Hernández, E.H. Falcão, Influence of graphene oxide and reduced graphene oxide on TiO2-reinforced flexible poly (vinyl alcohol) films for electromagnetic interference shielding, *Journal of Alloys and Compounds* 1010 (2025) 177671.

[2] Z. Zhang, Evolution and preparation of graphene oxide and deep learning image characterization, in: Journal of Physics: Conference Series, IOP Publishing, 2025: p. 012028. https://iopscience.iop.org/article/10.1088/1742-6596/2961/1/012028/meta (accessed April 6, 2026).

[3] A. Nadtochiy, A.M. Gorb, B.M. Gorelov, O. Polovina, O. Korotchenkov, Graphene-Based Polymer Nanocomposites: Models and Applications, Springer Nature Singapore, Singapore, 2024. https://doi.org/10.1007/978-981-97-2792-6.

[4] V. Pasindu, P. Yapa, S. Dabare, "I. Munaweera, Multifunctional transition metal oxide/graphene oxide nanocomposites for catalytic dye degradation, renewable energy, and energy storage applications" *RSC Advances 15* (2025) 33162–33186.

[5] O. Alami, R. Laurent, S. El Kazzouli, N. El Brahmi, A.-M. "Caminade, Dendrimers and graphene oxide: An overview on combination, properties and applications" *Coordination Chemistry Reviews* 558 (2026) 217781.

[6] J. Yang, J. Zhang, M. Yusoff, N.A. Roslan, M.H. "Razali, Titanium dioxide nanowires and reduced graphene oxide nanocomposite coated gellan gum film for drug delivery to enhance skin regeneration" *Digest Journal of Nanomaterials & Biostructures (DJNB)* 20 (2025). https://storage.imrpress.com/IMR/1972208059049676800/application/301-314.pdf (accessed April 6, 2026).

[7] M. Siahsahlan, S.M. Aref, H. Naghshara, R. "Azmayesh, The effects of reduced graphene oxide amount on the photocatalytic performance of TiO2 nanoparticles for hydrogen evolution" *International Journal of Hydrogen Energy* 142 (2025) 318–329.

[8] A.S. AlShammari, M.M. Halim, F.K. Yam, N.M. Kaus, "Synthesis of Titanium Dioxide (TiO2)/Reduced Graphene Oxide (rGO) thin film composite by spray pyrolysis technique and its physical properties" *Materials Science in Semiconductor Processing* 116 (2020) 105140.

[9] Y. Qiao, M. Li, Y. Zhao, X. Cheng, J. Chen, S. Yang, L. Ni, Y. Gong, S. Shi, "Stable dopamine-based ink for facile fabrication of robust and efficient fog-collectors" *Materials Today Chemistry* 42 (2024) 102345.

[10] R.P. Reshma, N.S. Abishek, K.N. "Gopalakrishna, Synthesis and characterization of gr aphene oxide, tin oxide, and reduced graphene oxide-tin oxide nanocomposites" *Inorganic Chemistry Communications* 165 (2024) 112451.

[11] J. Wei, X. Hu, Y. Li, Z. Bian, K. Yan, D. Wu, "3D-printed piezoelectric ceramics with auxetic structure for high-performance sensing applications" *Ceramics International* 51 (2025) 2509–2517.

[12] S. Li, S. Xia, X. Ma, L. Du, Y. Li, Z. Tang, Z. Wu, W. Zhang, "Graphene–Based Two-Dimensional Nanomaterials: From Scalable Synthesis" *Interfacial Mechanism to Emerging Biomedical Applications, Carbon Neutralization* 5 (2026) e70121. https://doi.org/10.1002/cnl2.70121.

[13] N. Rashidi, N.S. Harasymowicz, A. Savadipour, N. Steward, R. Tang, S. Oswald, "F. Guilak, PIEZO1-mediated mechanotransduction regulates collagen synthesis on nanostructured 2D and 3D models of fibrosis" *Acta Biomaterialia 193 (2025) 242–254*.

[14] B. Peng, X. Qi, L. Qiao, J. Lu, Z. Qian, C. Wu, Z. Xue, X. Kou, "Nanocomposite-Enabled Next-Generation food packaging: A comprehensive review on advanced Preparation Methods, functional Properties" *preservation Applications, and safety considerations, Foods 14 (2025) 3688.*

[15] M. Kigozi, B.N. Ezealigo, A.P. Onwualu, N.Y. Dzade, "Hydrothermal Synthesis of Metal Oxide Composite Cathode Materials for High Energy Application, in: F.I. Ezema, C.D. Lokhande, R. Jose (Eds.)" Chemically Deposited Nanocrystalline Metal Oxide Thin Films, Springer *International Publishing, Cham*, 2021: pp. 489–508. https://doi.org/10.1007/978-3-030-68462-4_19.

[16] J. Singh, D.D. Nguyen, P. Leclere, P. Nguyen-Tri, "Recent Advancements in Graphene-Based Nanocomposites for Enhanced Photocatalysis in Environmental Remediation: A Comprehensive Review" *Reviews Env.Contamination (Formerly:Residue Reviews)* 263 (2025) 13. https://doi.org/10.1007/s44169-025-00086-4.

[17] R. S. Yousif, "Examination of the structural, morphological, and self-cleaning characteristics of graphene oxide-based nanocomposite thin films," *Results in Physics*, p. 108410, 2025.

[18] Z.M. Talib, A.I. Hassan, J.A. Saimon, "Structural and optical properties of graphene-ZnO nanohybrid thin films synthesized by spray pyrolysis" *Journal of Applied Sciences and Nanotechnology* 2 (2022) 1–9.

[19] J.-D. Hwang and Z.-J. Hong, "Enhancing the Schottky-barrier height by inserting a thin MgO layer between Au and annealed-ZnO," *Materials Research Bulletin,* vol. 144, p. 111478, 2021.

[20] F. Bayati, M.K. Mohammadi, R.J. Yengejeh, A.A. Babaei, "Ag2O/GO/TiO2 composite nanoparticles: synthesis, characterization, and optical studies" *Journal of the Australian Ceramic Society* 57 (2021) 287–293.

[21] A. Piarristeguy, R. Nuernberg, D. Jouglard, M. Ramonda, R. Arinero, A. Pradel, M. Neyret," High-resolution electrical characterization of RuO2-borosilicate glass composites" *Journal of Alloys and Compounds* 876 (2021) 160123.

[22] N. Akhtar, M. Rani, A. Mahmood, K. Tariq, G. Murtaza, A.A. Alothman, R.S. AL-zahrani, S. Ali, N.K. Janjua, "A. Shah, Synthesis and characterization of graphene oxide-based nanocomposite NaCr2O4/GO for electrochemical applications" *Journal of Materials Research and Technology* 15 (2021) 6287–6294.

[23] T. Zinchenko, E. Pecherskaya, S. Gurin, M. Novichkov, V. Alexandrov, G. Kozlov, "Optimization of Deposition Parameters for Thin-Film Semiconductor Structures via Spray Pyrolysis" in: 2025 IEEE 26th *International Conference of Young Professionals in Electron Devices and Materials* (EDM), IEEE, 2025: pp. 130–134. https://ieeexplore.ieee.org/abstract/document/11096645/ (accessed April 7, 2026).